Stable closed-loop fiber-optic delay of arbitrary radio-frequency waveforms

A. Ben-Amram, Y. Stern, Y. London, Y. Antman, and A. Zadok*

Faculty of Engineering, Bar-Ilan University, Ramat-Gan 5290002, Israel
**Avinoam.Zadok@biu.ac.il*

Abstract: Thermal drifts in long fiber-optic delay lines are compensated based on chromatic dispersion. An arbitrary input radio-frequency (RF) waveform and a control RF sine wave modulate two different tunable laser sources and are coupled into the fiber delay line. The RF phase of the control tone at the output of the delay line is monitored and used to adjust the wavelengths of both sources, so that the effects of thermal drifts and dispersion cancel out. The input and control waveforms are separated in the optical domain, and no restrictions are imposed on their RF spectra. A figure of merit is proposed, in terms of the fiber delay, range of temperature changes that may be compensated for, and residual delay variations. An upper bound on performance is established in terms of the specifications of the tunable lasers. The principle is used in the stable distribution of sine waves and of broadband linear frequency-modulated (LFM) waveforms, which are commonly employed in radar systems. Lastly, the method is incorporated in stable interrogation of a localized hot-spot within a high-resolution, distributed Brillouin fiber sensing setup. The results demonstrate the applicability of the proposed protocol in the processing of arbitrary waveforms, as part of larger, more complex systems.

OCIS codes: (060.2360) Fiber optics links and subsystems; (060.2370) Fiber optics sensors; (060.5625) Radio frequency photonics.

References and links

1. J. Capmany and D. Novak, "Microwave photonics combines two worlds," Nat. Photonics **1**(6), 319–330 (2007).
2. J. Yao, ""A tutorial on microwave photonics, Part 2," IEEE Photonics Soc. News. **26**(2), 4–12 (2012).
3. A. M. Koonen, M. G. Larrode, A. Ng'oma, K. Wang, H. Yang, Y. Zheng, and E. Tangdiongga, "Perspectives of radio-over-fiber technologies," paper OThP3 in Proceedings of *Optical Fiber Communication Conference* (OFC 2008), Optical Society of America (2008).
4. W. Shillue, W. Grammer, C. Jacques, R. Brito, J. Meadows, J. Castro, Y. Masui, R. Treacy, and J.-F. Cliché, "The ALMA photonic local oscillator system," Proc. SPIE **8452**, 845216 (2012).
5. J. E. Román, L. T. Nichols, K. J. Wiliams, R. D. Esman, G. C. Tavik, M. Livingston, and M. G. Parent, "Fiber-optic remoting of an ultrahigh dynamic range radar," IEEE Trans. Microw. Theory Tech. **46**(12), 2317–2323 (1998).
6. D. T. K. Tong and M. C. Wu, "Multiwavelength optically controlled phased array antennas," IEEE Trans. Microw. Theory Tech. **46**(1), 108–115 (1998).
7. H. S. Choi, H. F. Taylor, and C. E. Lee, "High-performance fiber-optic temperature sensor using low-coherence interferometry," Opt. Lett. **22**(23), 1814–1816 (1997).
8. T. Horiguchi, T. Kurashima, and M. Tateda, "A technique to measure distributed strain in optical fibers," IEEE Photonics Technol. Lett. **2**(5), 352–354 (1990).
9. M. Niklès, L. Thévenaz, and P. A. Robert, "Simple distributed fiber sensor based on Brillouin gain spectrum analysis," Opt. Lett. **21**(10), 758–760 (1996).
10. K. Hotate and T. Hasegawa, "Measurement of Brillouin gain spectrum distribution along an optical fiber using a correlation-based technique -proposal, experiment and simulation," IEICE Trans. Electron **E83-C**(3), 405–412 (2000).
11. A. Zadok, Y. Antman, N. Primerov, A. Denisov, J. Sancho, and L. Thevenaz, "Random-access distributed fiber sensing," Laser Photonics Rev. **6**(5), L1–L5 (2012).
12. D. Elooz, Y. Antman, N. Levanon, and A. Zadok, "High-resolution long-reach distributed Brillouin sensing based on combined time-domain and correlation-domain analysis," Opt. Express **22**(6), 6453–6463 (2014).

#247446 Received 5 Aug 2015; revised 20 Sep 2015; accepted 7 Oct 2015; published 20 Oct 2015

13. A. Denisov, M. A. Soto, and L. Thévenaz, "1'000'000 resolved points along a Brillouin distributed fibre sensor," Proc. SPIE **9157**, 9157D2 (2014).
14. Y. London, Y. Antman, N. Levanon, and A. Zadok, "Brillouin analysis with 8.8 km range and 2 cm resolution," Proc. SPIE **9634**, 96340G (2015).
15. I. L. Newberg, C. M. Gee, G. D. Thurmond, and H. W. Yen, "Long microwave delay fiber optic link for radar testing," IEEE Trans. Micro. Theory Tech. **38**(5), 664–666 (1990).
16. J. M. Byrd, L. Doolittle, A. Ratti, J. W. Staples, and R. Wilcox, "Timing distribution in accelerators via stabilized optical fiber links," in *Proceeding of LINAC* (2006), pp. 577–579.
17. L. Zhang, L. Chang, Y. Dong, W. Xie, H. He, and W. Hu, "Phase drift cancellation of remote radio frequency transfer using an optoelectronic delay-locked loop," Opt. Lett. **36**(6), 873–875 (2011).
18. D. Hou, P. Li, C. Liu, J. Zhao, and Z. Zhang, "Long-term stable frequency transfer over an urban fiber link using microwave phase stabilization," Opt. Express **19**(2), 506–511 (2011).
19. A. Zhang, Y. Dai, F. Yin, T. Ren, K. Xu, J. Li, Y. Ji, J. Lin, and G. Tang, "Stable radio-frequency delivery by λ dispersion-induced optical tunable delay," Opt. Lett. **38**(14), 2419–2421 (2013).
20. A. Zhang, Y. Dai, F. Yin, T. Ren, K. Xu, J. Li, and G. Tang, "Phase stabilized downlink transmission for wideband radio frequency signal via optical fiber link," Opt. Express **22**(18), 21560–21566 (2014).
21. N. Levenon and E. Mozeson, *Radar Signals* (Wiley, 2004).
22. A. Ben-Amram, Y. Stern, and A. Zadok, "Fiber-optic distribution of arbitrary radio-frequency waveforms with stabilized group delay," in *CLEO 2015* (OSA, 2015), paper JTh2A.54.
23. A. Ben-Amram, Y. Stern, Y. London, Y. Antman, and A. Zadok, "Stabilized fiber-optic delay of arbitrary waveforms with application in distributed sensors," in *IEEE Conference on Microwave Photonics (MWP)* (IEEE, 2015).
24. J. Wang and K. Petermann, "Small signal analysis for dispersive optical fiber communication systems," J. Lightwave Technol. **10**(1), 96–100 (1992).
25. R. Rotman, O. Raz, and M. Tur, "Small signal analysis for analogue optical links with arbitrary optical transfer function," Electron. Lett. **40**(8), 504–505 (2004).
26. R. Rotman, O. Raz, and M. Tur, "Analysis of a true time delay photonic beamformer for transmission of a linear frequency-modulated waveform," J. Lightwave Technol. **23**(12), 4026–4036 (2005).
27. A. Zadok, O. Raz, A. Eyal, and M. Tur, "Optically controlled low distortion delay of GHz-wide RF signals using slow light in fibers," IEEE Photonics Technol. Lett. **19**(7), 462–464 (2007).
28. A. Zadok, A. Eyal, and M. Tur, "GHz-wide optically reconfigurable filters using stimulated Brillouin scattering," J. Lightwave Technol. **25**(8), 2168–2174 (2007).
29. L. Yaron and M. Tur, "RF nonlinearities in an analog optical link and their effect on radars carrying linear and nonlinear frequency modulated pulses," J. Lightwave Technol. **30**(22), 3475–3483 (2012).
30. R. W. Boyd, *Nonlinear Optics*, 3rd Edition, (Academic, 2008).
31. K. Y. Song, Z. He, and K. Hotate, "Distributed strain measurement with millimeter-order spatial resolution based on Brillouin optical correlation domain analysis," Opt. Lett. **31**(17), 2526–2528 (2006).
32. Y. Antman, N. Levanon, and A. Zadok, "Low-noise delays from dynamic Brillouin gratings based on perfect Golomb coding of pump waves," Opt. Lett. **37**(24), 5259–5261 (2012).

1. Introduction

The distribution of radio-frequency (RF) and microwave signals over long optical fibers is used to extend the reach and coverage of cellular networks [1–3]. Compared with RF coaxial cables, radio-over-fiber links benefit from the low propagation losses, ultra-broadband transmission bandwidth and immunity to electro-magnetic interference provided by fibers [1]. Fibers are also employed in the distribution of high-frequency local oscillators in large antenna arrays of radio-astronomy observatories [4], separation between a central unit of a radar system and remote antennas [5], emulation of long-distance targets, testing and calibration of radar systems, and beam-forming within phased-array antennas [6].

The group delay along an optical fiber drifts with temperature by approximately 7.5 ppm per °C, due to the thermo-optic effect and thermal expansion in silica [7]. Many precision applications of microwave photonics cannot tolerate such delay variations. For example, the RF phase of oscillators distributed over fiber can become arbitrary, and the beams transmitted by phased-array antennas might become spatially-distorted. In addition to the above more traditional applications, the need for stable delay recently emerged in setups for high-resolution distributed fiber sensors of temperature and strain [8,9]. Phase-coded Brillouin optical correlation-domain analysis (phase-coded B-OCDA) protocols rely on the modulation of the counter-propagating Brillouin pump and signal waves with high-rate phase codes, so that their complex envelopes are in correlation only within discrete and narrow peak positions of interest [10–14]. Brillouin scattering is effectively stimulated in these locations only [10].

#247446 Received 5 Aug 2015; revised 20 Sep 2015; accepted 7 Oct 2015; published 20 Oct 2015

Using this scheme, distributed measurements were performed along many km of fiber with cm-scale resolution [13,14]. However, the scanning of correlation peaks positions involves the distribution of the modulated waveforms over long fiber delay lines, up to 50 km length in some embodiments. The delay of these waveforms must be stable to within 1-2 cm over 1-2 hours.

Previous attempts to overcome thermal drifts in fiber delay lines included passive thermal isolation [15], phase-locked loops [16,17], and compensation based on digital signal processing [18]. However, these solutions either provide insufficient stabilization or are too complicated and unsuitable for incorporation in radar and sensor systems. Recently, Zhang and associates proposed the compensation of thermal delay drifts using chromatic dispersion [19,20]. An input RF waveform and an internal control sine wave jointly modulated the output of a single tunable laser. Following propagation along the fiber, the two waveforms were detected and separated by RF filters. The output phase of the control tone was then monitored and used to drive a feedback loop and adjust the source wavelength, so that the effects of thermal drift and chromatic dispersion canceled out [19,20]. This method required, however, that the RF spectra of the control tone and of the input waveform did not overlap. This requirement is difficult to accommodate in systems that make use of broadband waveforms, such as high-resolution Brillouin analysis setups in which phase coding rates reach 12 Gbit/s [11], and any distortion due to RF-filtering degrades the measurements.

In this work we propose, demonstrate and employ an extended delay stabilization scheme, in which the control tone and the broadband input waveform modulate separate tunable laser sources of different wavelengths. The RF phase of the control tone is tracked and used to correct the wavelengths of both sources. The separation between the two waveforms is carried out in the optical domain, so that all restrictions on the RF spectra of the two signals are removed. An extended analysis of the compensation principle is provided, and a system figure of merit is proposed in terms of the extent of delay, residual delay variations, and range of temperature changes that may be accommodated. An upper bound on system performance is established, in terms of the properties of the tunable laser sources used.

Using the proposed method, a 3 GHz sine wave is distributed over 18 km of fiber with residual delay variations of ± 4 ps (or ± 0.05 ppm). We also demonstrate the distribution of broadband linear frequency-modulated (LFM) waveforms, which are widely employed in radar systems [21], over 9 km of fiber. Residual delay drifts of these waveforms are reduced from 200 ps in a free-running delay line to 20 ps under closed-loop operation, limited by the timing jitter of our sampling equipment in the acquisition of long traces. Lastly, the method is also employed in high-resolution distributed fiber sensing measurements. The temperature of a local, 2 cm-wide hot-spot was correctly monitored, while a 25 km-long delay line incorporated in the setup had undergone thermal drifts that were several times larger. A free-running experiment in similar conditions resulted in erroneous interrogation. Preliminary results were briefly reported in [22,23].

2. Principle of operation

2.1 Compensation of thermal delay drifts using chromatic dispersion

Consider a tunable laser source of wavelength λ, coupled into a fiber delay line of length L. The group delay index of the fiber is $n(\lambda)$, and its chromatic dispersion coefficient is $D(\lambda)$ [in units of ps/(nm × km)]. The group delay along the fiber, $\tau = nL/c$, varies with changes ΔT in the surrounding temperature T according to:

$$\Delta\tau_T = \left(\frac{1}{n}\frac{\partial n}{\partial T} + \frac{1}{L}\frac{\partial L}{\partial T}\right)\frac{n}{c}L\cdot\Delta T = \left(\frac{1}{n}\frac{\partial n}{\partial T} + \frac{1}{L}\frac{\partial L}{\partial T}\right)\tau\cdot\Delta T \equiv \alpha_\tau\tau\cdot\Delta T. \qquad (1)$$

#247446 Received 5 Aug 2015; revised 20 Sep 2015; accepted 7 Oct 2015; published 20 Oct 2015

In Eq. (1), $\alpha_n \equiv (1/n)(\partial n/\partial T)$ = 7 ppm/°C is the thermo-optic coefficient of the fiber [7], $\alpha_L \equiv (1/L)\cdot(\partial L/\partial T)$ = 0.5 ppm/°C denotes the linear thermal expansion coefficient [7], and $\alpha_\tau \equiv (1/\tau)\cdot(\partial \tau/\partial T) = \alpha_n + \alpha_L$. Although variations of τ with λ accumulate significantly over many km of fiber, we may neglect the wavelength dependence of small-scale thermal delay drifts. Therefore we consider $\Delta\tau_T$ as wavelength-independent.

Thermally-induced variations in group delay may be cancelled out based on chromatic dispersion [19,20]. Changes $\Delta\lambda$ to the source wavelength λ induce group delay variations according to:

$$\Delta\tau_D(\lambda) = D(\lambda)L\cdot\Delta\lambda = \frac{c}{n}D(\lambda)\tau\cdot\Delta\lambda. \tag{2}$$

Perfect cancellation may be achieved with the proper choice of wavelength offsets:

$$\Delta\lambda(\lambda) = -\frac{n}{cD(\lambda)}\alpha_\tau\Delta T. \tag{3}$$

Zhang *et al.* had proposed to modulate the output of a single tunable laser of wavelength λ_1 by the input RF waveform, mixed together with a control sine wave of radio frequency f [19,20]. Part of the light is detected at the far end of the delay fiber, where the input waveform is filtered in the RF domain for further use. A fraction of the optical waveform is reflected back to the transmitter end, where it is detected and filtered to select the control tone. Thermal drift in the two-way group delay leads to a variation in the RF phase of the sine wave:

$$\Delta\varphi_{1T} = 2\pi f\cdot 2\Delta\tau_T. \tag{4}$$

Hence the tracking of $\Delta\varphi_{1T}$ provides the necessary feedback for estimating $\Delta\tau_T$ and adjusting the wavelength of the laser source in a closed loop. A wavelength offset $\Delta\lambda_1$ induces an additional variation to the RF phase of the delayed control tone: $\Delta\varphi_{1D} = 2\pi f\cdot 2\Delta\tau_D$, which can be tuned to cancel out $\Delta\varphi_{1T}$ (and thereby $\Delta\tau_T$):

$$\Delta\varphi_{1D} = -\Delta\varphi_{1T} \Rightarrow \Delta\lambda_1 = -\frac{\Delta\tau_T}{LD(\lambda_1)} = -\frac{\Delta\varphi_{1T}}{2\pi f\cdot 2LD(\lambda_1)}. \tag{5}$$

Residual phase variations may be identified by mixing the reconstructed RF sine wave with a replica of itself, which was retained at the transmitter end and not delayed along the fiber. Mixing products at frequency $2f$ are filtered out. The DC voltage term at the mixer output can be written as:

$$V = V_0\cos(\Delta\varphi_{1B} + \Delta\varphi_{1T} + \Delta\varphi_{1D}). \tag{6}$$

Here V_0 denotes a maximum voltage, obtained when the delayed and reference RF tones are in-phase. Its value depends on the optical power level of the laser source, losses along the fiber, the responsivity of the photo-detector, and on parameters of the mixer. V_0 is therefore calibrated experimentally. $\Delta\varphi_{1B}$ represents an arbitrary bias in the phase difference between the two tones.

The feedback protocol is set to maintain an arbitrarily chosen reference voltage level $-V_0 \le V_{ref} \le V_0$. Residual phase variations in $\Delta\varphi_{1T} + \Delta\varphi_{1D}$ would manifests as small-scale deviations of the output voltage from V_{ref}. For convenience we choose $V_{ref} = 0$, which implies $\Delta\varphi_{1B} = -\pi/2$. Subject to that choice, and for small residual phase drifts $\Delta\varphi_{1T} + \Delta\varphi_{1D} << 2\pi$, we have:

#247446 Received 5 Aug 2015; revised 20 Sep 2015; accepted 7 Oct 2015; published 20 Oct 2015

$$V = V_0 \sin\left(\Delta\varphi_{1T} + \Delta\varphi_{1D}\right) \approx V_0\left(\Delta\varphi_{1T} + \Delta\varphi_{1D}\right). \tag{7}$$

A sufficient loop bandwidth would guarantee that variations in $\Delta\varphi_{1T} + \Delta\varphi_{1D}$ remain small, in agreement with the above condition. Using Eq. (5) and Eq. (7), the necessary correction to the wavelengths λ_1 is directly obtained from the voltage reading at the mixer output:

$$\Delta\lambda_1 = -\frac{1}{2\pi f \cdot 2LD(\lambda_1)}\frac{V}{V_0} \equiv -\alpha_{\lambda 1} V. \tag{8}$$

In this work, we propose the following extension of the delay stabilization principle: Rather than superimpose the input RF waveform to be delayed together with the control sine wave onto the same optical carrier of wavelength λ_1, we use a separate laser source of wavelength $\lambda_2 \neq \lambda_1$ for that purpose. In doing so, we may separate between the input waveform and the control tone directly in the optical domain. Such separation is advantageous when the input waveform is broadband. The feedback that is provided in measurements of V may also serve for the adjustments in wavelength λ_2:

$$\Delta\lambda_2 = -\frac{1}{2\pi f \cdot 2LD(\lambda_2)}\frac{V}{V_0} = -\frac{D(\lambda_1)}{D(\lambda_2)}\alpha_{\lambda 1} V \equiv -\alpha_{\lambda 2} V. \tag{9}$$

Due to dispersion slope in standard fibers, differences between $\alpha_{\lambda 1}$ and $\alpha_{\lambda 2}$ across the C-band wavelength range can be as large as 20%. These must be taken into account. Adjustments according to Eq. (8) and Eq. (9) guarantee that the group delays at the two wavelengths, although different, both remain stable.

2.2 Figure of merit and performance limitations

Errors $\delta\lambda$ in the setting of wavelengths induce delay variations $\delta\tau$. An inherent tradeoff exists in the choice of fiber dispersion: large values of D would support the compensation of thermal drifts over a broad temperature range $\Delta T_{\max}$, however smaller dispersion coefficients would reduce $\delta\tau$. This trade-off can be quantified in terms of the following figure of merit, using Eq. (2) and Eq. (3):

$$\mathrm{FoM} \equiv \frac{\tau}{\delta\tau}\Delta T_{\max} = \frac{\tau}{LD\cdot\delta\lambda}\frac{cD}{n\alpha_\tau}\Delta\lambda_{\max} = \frac{1}{\alpha_\tau}\frac{\Delta\lambda_{\max}}{\delta\lambda} \equiv \frac{1}{\alpha_\tau}N_\lambda. \tag{10}$$

Here $\Delta\lambda_{\max}$ is the tuning range of the laser source. The units of FoM are °C. Note that the dispersion coefficient cancels out of the figure of merit. It can be chosen to emphasize a particular metric of the fiber-optic delay line, but only at the expense of others. Equation (10) highlights the significance of the effective number of wavelength resolution points: $N_\lambda \equiv \Delta\lambda_{\max}/\delta\lambda$, in setting an upper bound on the performance of the stabilized fiber delay line. Wavelength fluctuations might be inherent to the laser sources, but could also stem from noise in voltage readings or from a limited feedback bandwidth.

The RF bandwidth of the input waveform is restricted by dispersion-induced fading. Assuming double-sideband, small-signal amplitude modulation, one can show that the 3 dB RF bandwidth of delayed distribution is given by [24,25]:

$$f_{3dB} = \frac{1}{2\pi}\sqrt{\frac{\pi}{3|\beta_2|L}} = \frac{1}{2\lambda}\sqrt{\frac{2n}{3|D|\tau}} \approx \frac{1}{2\lambda\sqrt{|D|\tau}}. \tag{11}$$

Here $\beta_2 = -\lambda^2 D/(2\pi c)$, in units of ps^2/km. The bandwidth limitation for a 25 km-long, standard single-mode fiber delay line is about 7 GHz.

#247446 Received 5 Aug 2015; revised 20 Sep 2015; accepted 7 Oct 2015; published 20 Oct 2015

3. Experimental setup and results

3.1 Experimental setup

Figure 1 shows the experimental setup for the stabilized distribution of arbitrary RF waveforms using two laser sources. Light from an external-cavity, tunable laser diode source was modulated by a sine wave at 3 GHz frequency, using an external electro-optic amplitude modulator. The wavelength λ_1 of that source could be continuously adjusted between 1530 and 1565 nm by changing the external cavity length. The output of a second source, comprised of an array of distributed feedback laser diodes, was modulated by a user's input RF signal, (such as an LFM waveform), using a second external modulator. The wavelength λ_2 of the second source could be scanned continuously across a 2 nm-wide range by changing the temperature and/or drive current of individual diodes. The entire range of 1530-1565 nm could be scanned piece-wise through switching between different diodes. The two optical waveforms were coupled into a 9 km-long standard fiber, having a chromatic dispersion coefficient of 17 ps/(nm × km) at 1550 nm and a dispersion slope of 0.092 ps/(nm^2 × km).

Light at the far end of the delay line was split in two paths. The waveforms in one arm were reflected back towards the transmitter end by a fiber mirror. Light in the second output branch was filtered by an optical band-pass filter to keep hold of λ_2 only, and detected to recover a delayed replica of the input waveform. The output waveform was sampled by a real-time digitizing oscilloscope for display or further processing, as necessary.

Following two-way propagation back to the near end of the fiber delay, the optical waveforms were directed by a fiber-optic circulator to a second optical band-pass filter, which retained only λ_1. The control sine wave was directly detected and mixed with a replica of itself, which was kept at the transmitter end, using a RF mixer. The electrical mixing efficiency is not affected by the state of polarization of the delayed control tone. A low-pass filter (not shown) was applied at the mixer output to block-off all high-frequency terms. The resulting DC voltage V was sampled by a computer-controlled interface, and used to adjust the wavelengths of both tunable lasers according to Eq. (8) and Eq. (9) through digital commands. Wavelengths corrections were applied every 0.5 s. The maximum voltage value V_0, necessary for setting the scaling factors $\alpha_{\lambda 1,\lambda 2}$, was calibrated by sweeping λ_1 and observing the mixer output in free-running operation. V_0 was on the order of 100-200 mV throughout the experiments reported below.

#247446 Received 5 Aug 2015; revised 20 Sep 2015; accepted 7 Oct 2015; published 20 Oct 2015

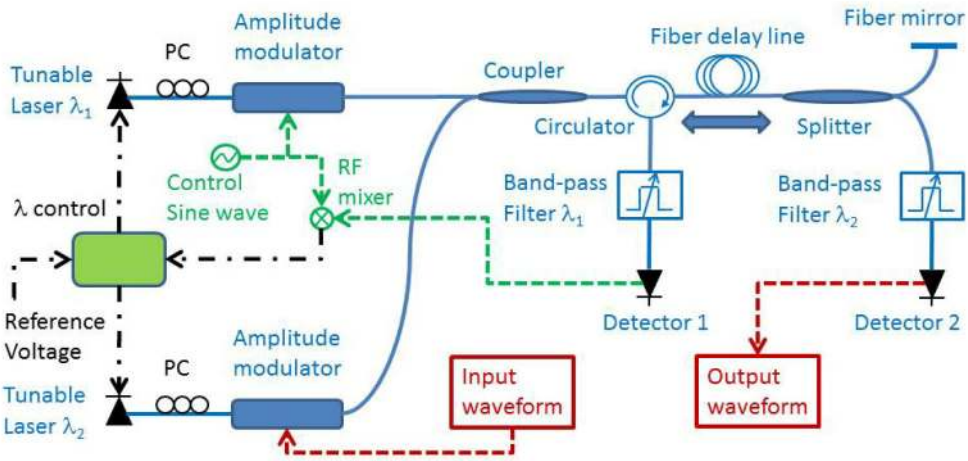

Fig. 1. Experimental setup for the stabilized delay of arbitrary input RF waveforms based on chromatic dispersion, using two tunable laser sources. Blue, solid lines: fiber-optic paths. Green, dashed lines: RF paths of the control tone. Red, dashed lines: RF paths of the input waveform. Black, dashed-dotted lines, DC control signals. PC: polarization controller [22].

Residual delay variations stem from uncertainties in both the setting of wavelengths and in the measurement of voltage. The wavelength setting error $\delta\lambda$ in λ_1 was ± 30 pm, corresponding to $\delta\tau$ of about ± 5 ps over 9 km. The standard deviation of the noise δV in voltage measurements was on the order of ± 5 mV, corresponding to delay variations $\delta\tau = \delta V/(2\pi f V_0)$ on the order of ± 2.5 ps. Polarization mode dispersion over the relevant lengths of fiber is negligible with respect to the above delay uncertainties.

Thermal delay drifts within the laboratory environment were accelerated in some experiments by placing a halogen lamp in the vicinity of the delay fiber. Even so, the rate of delay drift was rather slow: at most 3 ps per second. Therefore, delay variations within the sampling interval of the feedback loop were below the delay uncertainty imposed by wavelength setting errors. Although the feedback bandwidth was very narrow (2 Hz), it was nevertheless sufficient to compensate for thermal drifts, as demonstrated next.

3.2 Stable distribution of radio-frequency sine waves

The stable distribution of RF sine waves based on chromatic dispersion and wavelength tuning had been successfully demonstrated [19,20]. It is repeated here briefly for validation and illustration purposes, and for estimating residual delay variations. The second laser source at λ_2 was not used in this stage. Figure 2 shows persistence traces of the 3 GHz control tone, following two-way propagation along the delay fiber. Each measurement was taken over 10 minutes, while the delay fiber was deliberately heated. The RF phase of the delayed sine wave, subject to free-running operation, becomes entirely random. The application of wavelength feedback leads to a stable output phase. The Residual variations in the closed-loop delay were ± 4 ps, in line with expectations. These residual delay drifts are equivalent to those induced by temperature fluctuations of ± 0.006 °C.

#247446 Received 5 Aug 2015; revised 20 Sep 2015; accepted 7 Oct 2015; published 20 Oct 2015

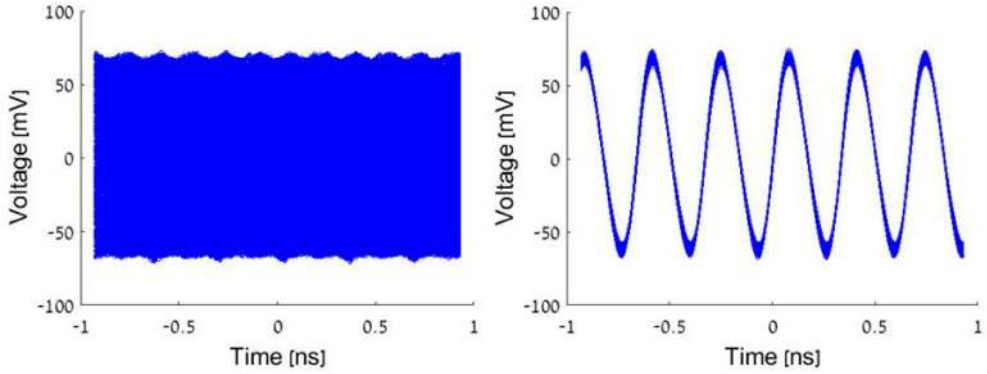

Fig. 2. Persistence traces of a 3 GHz control sine wave, following two-way propagation along 9 km of fiber. Left – free-running delay. Right – closed-loop delay.

Figure 3(left) shows the mixer voltage readings V as a function of time. Drift over more than a full period is observed during free-running operation (first ten minutes), whereas a stable value near zero is maintained by closing the loop (final ten minutes). Figure 3(right) shows the instantaneous setting of λ_1. The wavelength was continuously adjusted during closed-loop operation in the final ten minutes, to maintain a stable delay.

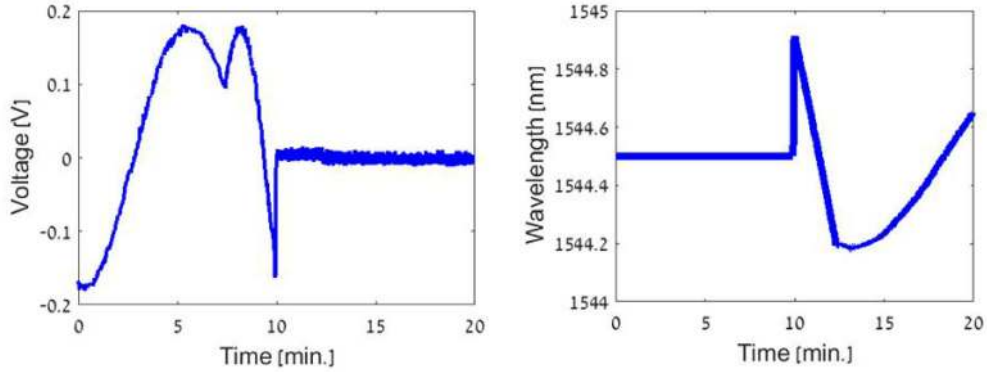

Fig. 3. Left - output DC voltage obtained in the mixing of a delayed 3 GHz sine wave and a non-delayed replica, as a function of time. The delay line was free-running in the first ten minutes of the experiment, and the feedback loop was closed in the final ten minutes. Right - wavelength of the tunable laser source of control channel λ_1 as a function of time, during the same measurement. The wavelength was not modified in the first ten minutes of the measurements, and was continuously adjusted during closed-loop operation over the final ten minutes, to maintain a stable delay.

3.3 Stable distribution of broadband, linear frequency-modulated radar waveforms

The instantaneous magnitude of an LFM waveform of bandwidth B, central frequency f_0 and duration T_{LFM} can be written as [21]:

$$A(t) = A_0 \cos\left(2\pi f_0 t + \pi \frac{B}{T_{LFM}} t^2\right) \mathrm{rect}\left(\frac{t}{T_{LFM}}\right). \tag{12}$$

Here A_0 is a constant magnitude, and $\mathrm{rect}(x) = 1$ for $|x| \le 0.5$ and zero elsewhere. The correlation of $A(t)$ with a replica of itself effectively compresses the entire energy of the

#247446 Received 5 Aug 2015; revised 20 Sep 2015; accepted 7 Oct 2015; published 20 Oct 2015

extended waveform to a virtual peak of width $\Delta T_{LFM} \approx 1/B << T_{LFM}$. LFM waveforms are widely employed in radar systems, where they provide both high ranging resolution and high signal to noise ratios in the detection of echoes. The constant magnitude of the waveforms makes them comparatively simple to generate and process. Due to their practical significance, LFM waveforms are often used to test and characterize microwave photonic setups [26–29].

In a second stage of the experiment, an LFM waveform with 500 MHz bandwidth, central frequency of 1.75 GHz and duration of 5 μs was used as an input waveform, modulating the laser source of wavelength λ_2 (see Fig. 1). The delayed waveform at the output of the 9 km-long delay fiber was detected, sampled and compressed using off-line correlation processing. The continuous tuning range of the laser source λ_2 ($\Delta\lambda_{\max}$) was only 2 nm, therefore the largest delay variations that could be accommodated were about 300 ps.

Figure 4 shows persistence traces of the compressed waveforms following one-way delay, acquired every 5 s over 2 minutes. The width of the main lobe of the compressed traces is 2 ns, as expected. The timing of the main peak drifts over 200 ps in free-running operation, whereas residual timing fluctuations are restricted to 20 ps in closed-loop operation. The timing inaccuracy of the sampling oscilloscope is specified as about ± 1 ppm of the acquisition trace duration. Timing errors in the sampling of long LFM waveforms therefore reach ± 10 ps.

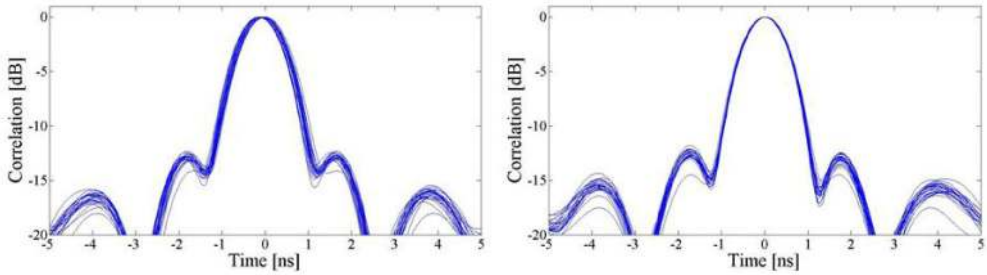

Fig. 4. Persistence traces of compressed LFM waveforms, sampled at the output of a 9 km-long fiber-optic delay line every 5 s, over 2 minutes. The central frequency, bandwidth and duration of the waveforms were 500 MHz, 1.75 GHz and 5 μs, respectively. The main lobe of the compressed waveform is 2 ns wide. Left – free-running delay line. Right – closed-loop operation. Delay drifts are reduced from 200 ps to 20 ps in closed-loop operation.

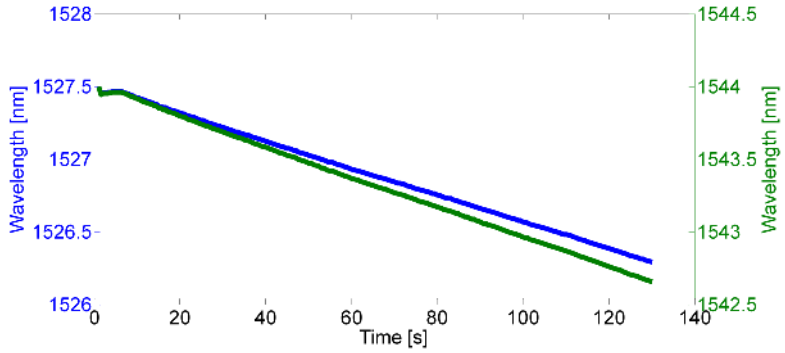

Fig. 5. Wavelengths of the tunable laser sources as a function of time: control channel λ_1 (blue trace, left-hand axis), and channel of the LFM waveform λ_2 (green trace, right-hand axis), during closed-loop operation.

#247446 Received 5 Aug 2015; revised 20 Sep 2015; accepted 7 Oct 2015; published 20 Oct 2015

Figure 5 shows the settings of $\lambda_{1,2}$ as a function of time, during closed-loop operation. Both wavelengths were tuned over about 1.25 nm. The corresponding variation in group delay is 190 ps. The traces suggest that the fiber was heated at a nearly constant rate.

4. Stable interrogation of a local hot spot in high-resolution distributed Brillouin analysis

4.1 Brillouin optical correlation-domain analysis principles

The following subsection provides a brief introduction to B-OCDA. Full detail is found in the references that are mentioned below. In Brillouin analysis setups, pump and signal waves are launched into a fiber under test in opposite directions. The amplification of the signal wave is measured as a function of position z along the fiber, and experiments are repeated over multiple values of the frequency offset ν between pump and signal [8,9]. The frequency offset of maximum gain, known as the Brillouin frequency shift $\nu_B(z)$, is identified in each location using post-processing analysis. The value of ν_B in standard fibers and at 1550 nm wavelength is on the order of 11 GHz. The Brillouin shift varies, however, with both local temperature and local mechanical strain [8,9]. Hence Brillouin analysis is being used in the distributed sensing of both quantities for 25 years.

The key to high spatial resolution in Brillouin analysis is careful control over where and when the interaction between the two optical waves is effectively stimulated. The optical waves are coupled by a mediating acoustic field, which is stimulated, in turn, by the very same waves [30]. One can show that the magnitude of the acoustic field at a given location is closely related to the temporal cross-correlation function between the complex envelopes of pump and signal waves at that location [10–14]. In B-OCDA protocols, the two waves are modulated so that their correlation is confined to discrete and narrow peaks. The Brillouin interaction is effectively stimulated within these locations only, providing high resolution measurements [10,31].

A recently-proposed, efficient variant of B-OCDA involves the coding of both optical waves by a repeating, high-rate phase sequence with symbol duration T_s and a period of N_s bits [11–14]. A large number of correlation peaks are typically introduced, with a spatial extent of $\Delta z = \frac{1}{2}(c/n)T_s$ (which also signifies resolution), and separation between neighboring peaks of $N_s \cdot \Delta z$ [11–14]. Post-detection data analysis protocols are able to simultaneously and unambiguously interrogate Brillouin interactions taking place at thousands of correlation peaks [12–14]. One of the main challenges in the realization of phase-coded B-OCDA is the spatial scanning of correlation peaks positions. The favored solution path to-date relies on long fiber delay lines, as discussed next.

4.2 Experimental setup and results

Figure 6 shows a schematic illustration of a phase-coded B-OCDA setup, which also includes a delay line that is stabilized based on the principles of this work. The tunable laser source at wavelength λ_2, discussed in previous sections, is used as the common source for Brillouin pump and signal waves. The analysis protocol follows that of [12]: Light from the laser output is phase-modulated by a repeating binary sequence (N_s = 211 bits), chosen for its favorable correlation properties [32]. The symbol duration T_s of 200 ps corresponds to Δz of 2 cm.

The modulated light is split into pump and signal branches, that are linked through a 200 m long fiber under test to form a fiber loop. The value of ν_B in the fiber under test at room temperature is 10.85 GHz. Light in the pump branch is offset in frequency by an adjustable ν using an electro-optic single-sideband modulator, restricted to repeating, 20 ns-long pulses by an electro-optic amplitude modulator, and amplified by an erbium-doped fiber amplifier.

#247446 Received 5 Aug 2015; revised 20 Sep 2015; accepted 7 Oct 2015; published 20 Oct 2015

These components are not shown in Fig. 6, for better clarity and focus on the current work (see [12] for full detail). Light in the signal branch passes through a 25 km-long delay fiber and enters the fiber under test from the opposite direction. The signal wave at the output of the fiber under test is filtered by an optical band-pass filter that retains λ_2, detected by a photo-receiver, and sampled for off-line processing.

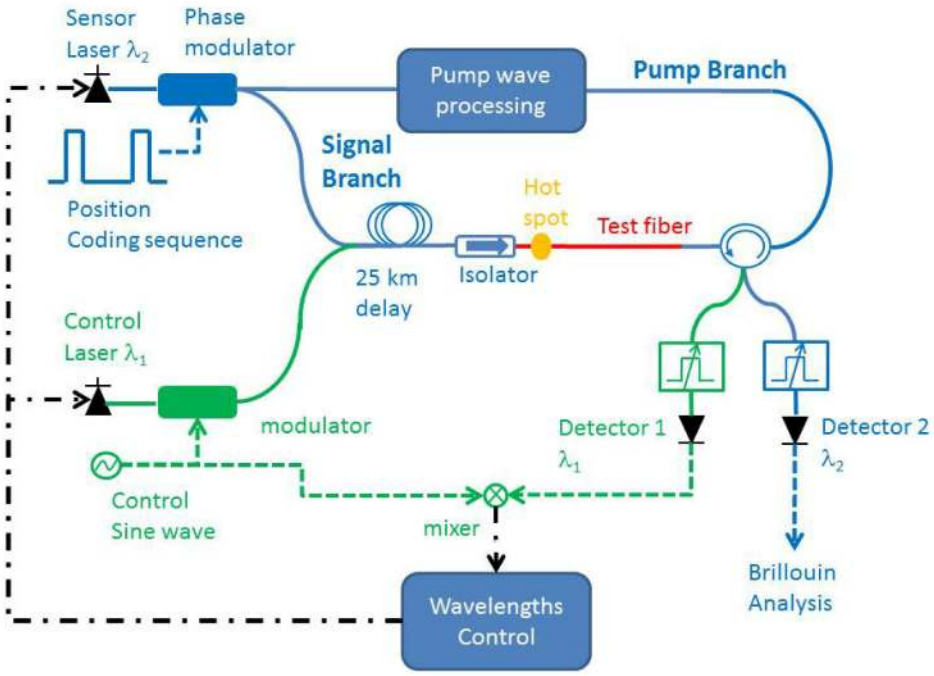

Fig. 6. Schematic illustration of a phase-coded Brillouin optical correlation-domain analysis setup, incorporating a stabilized fiber-optic delay line in the path of the Brillouin signal wave. Solid lines denote fiber paths, dashed lines represent RF cable paths, and dashed-dotted, black lines correspond to DC control signals. Blue color represents paths and components related to the sensing functionality, whereas green paths and components are part of the delay stabilization module. Details of the 'Pump wave processing' module are not shown, for better clarity (see [12]).

The role of the long fiber delay is as follows: The middle of the fiber loop is defined as the location of equal distances from the splitting point at the phase modulator output (see Fig. 6), going in clockwise and counter-clockwise directions. Correlation peaks are introduced at distances $Z_m = m \cdot N_s \cdot \Delta z = \frac{1}{2} m \cdot N_s \cdot (c/n) T_s$ from the middle of the loop, where m is an integer. The locations Z_m of all peaks, with the exception of the zero-order one, may therefore be moved with slight changes ΔT_s to the symbol duration: $\Delta Z_m / Z_m = \Delta T_s / T_s$.

Let us denote the highest (lowest) order of correlation peaks in overlap with the fiber under test as $m_{\max}$ ($m_{\min}$). A sufficiently long delay imbalance in the signal path guarantees that $(m_{\max} - m_{\min}) << m_{\min}$. Consequently, the positions of all correlation peaks can be scanned with practically equal increments, which are set to match the resolution step: $\Delta Z_m \approx \Delta z$ for all $m_{\min} < m < m_{\max}$. The long fiber delay allows for the rapid, all-electrical scanning of correlation peak positions, with no moving parts and over long ranges [11].

The proper function of the sensing setup requires that the long fiber delay remains stable to within $\frac{1}{2} T_s$ throughout the duration of the analysis, which might require 1-2 hours.

#247446 Received 5 Aug 2015; revised 20 Sep 2015; accepted 7 Oct 2015; published 20 Oct 2015

Stabilization was achieved using the protocol proposed in this work. Light from a laser diode source of wavelength λ_1 was modulated by a 3 GHz control sine wave and coupled into the signal path (see Fig. 6). The control channel was filtered and detected at the output of the fiber under test, and the RF phase of the reconstructed sine wave was used to adjust both λ_1 and λ_2 as discussed above. In order to test the stability of the setup, a 2 cm-wide hot-spot was introduced at an arbitrary location along the fiber under test, and T_s was fine-tuned so that one of the correlation peaks was in overlap with the hot-spot. The Brillouin gain spectrum at that position was then repeatedly acquired every 30 s, while the 25 km-long delay line was heated.

First, feedback was applied to the control laser wavelength λ_1 only, while the sensor laser wavelength λ_2 remained fixed and the thermal drifts of the Brillouin signal wave were not compensated for. Figure 7(bottom) shows the instantaneous setting of λ_1. Intentional heating of the delay line began six minutes into the measurements. Starting at that stage, the wavelength was adjusted over a 1.2 nm range (left-hand axis), indicating a thermal drift in path length of over 10 cm (right-hand axis). Figure 7(top) shows the Brillouin gain spectra as a function of time. Ten minutes into the experiment, the measured gain spectrum was shifted from that of the hot-spot to that of the fiber under test at room temperature. Thermal delay drift therefore led to an incorrect interpretation of the measurement data.

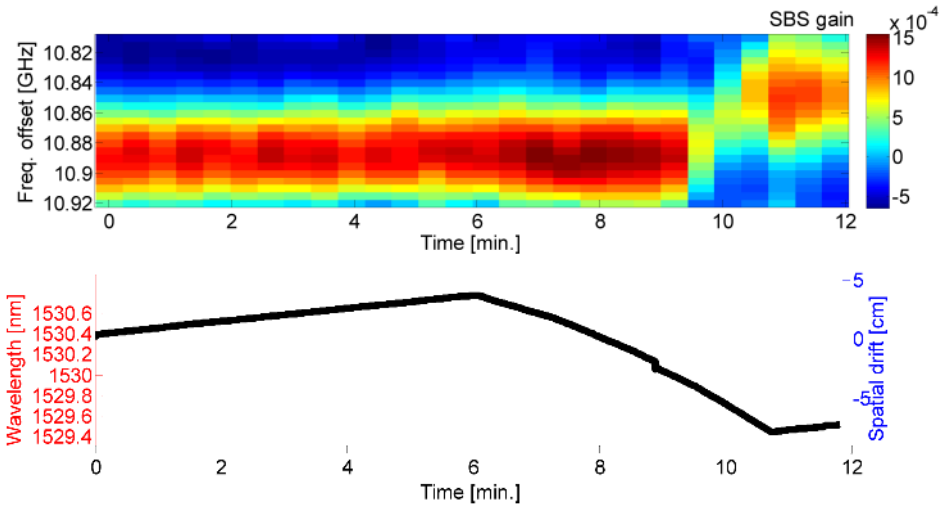

Fig. 7. Top – Measured Brillouin gain as a function of frequency offset between pump and signal, and of time. The phase-coded B-OCDA setup was adjusted to monitor the Brillouin gain spectrum in a 2 cm-wide hot-spot. The delay of the Brillouin signal was free-running, without closed-loop feedback to the wavelength of the sensor laser. The Brillouin gain spectrum changed after 10 minutes, from that of the hot-spot to that of the fiber under test at room temperature. Bottom – Wavelength of the control channel λ_1 (left-hand axis), and the implied thermal drift in the path length of the 25 km-long delay line (right-hand axis), as a function of time. Thermal drift on the order of 10 cm is observed. SBS: stimulated Brillouin scattering.

In a second experiment, closed-loop feedback was applied to the wavelength of the sensor laser λ_2 as well. Figure 8(bottom) shows the settings of that wavelength as a function of time. Here too, heating of the delay line started after six minutes, and the wavelength changes indicate a thermal drift of about 9 cm, or several times larger than both Δz and the extent to the hot-spot. This time, however, the measured Brillouin gain spectrum remained that of the

#247446 Received 5 Aug 2015; revised 20 Sep 2015; accepted 7 Oct 2015; published 20 Oct 2015

hot-spot (see top panel). Lastly, Fig. 9 shows the experimentally estimated ν_B as a function of time, for both experiments. The instantaneous adjustments to λ_2 are accounted for in the data analysis of the second experiment, as ν_B is inversely proportional to the optical wavelength [30]. The stabilization of the delay line allowed for correct interrogation of the narrow hot-spot in the presence of thermal drift. Note that the temperature of the hot-spot was not the same in the two experiments.

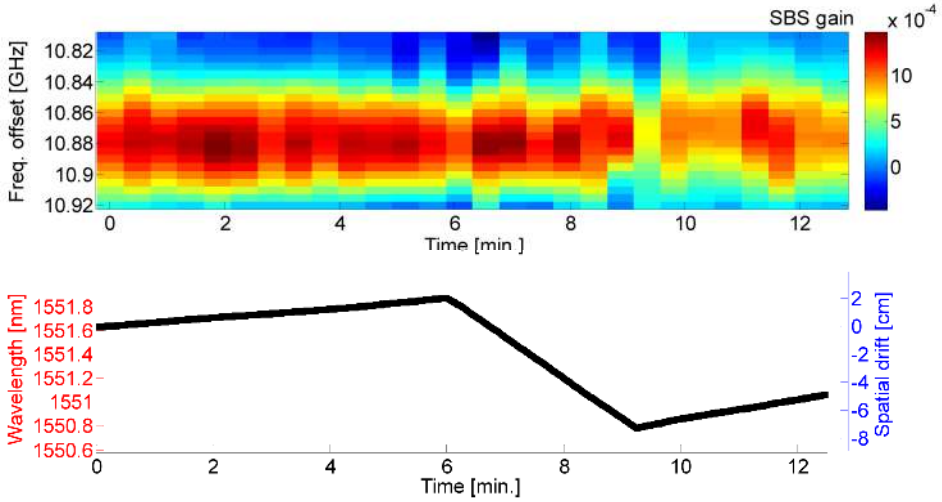

Fig. 8. Top – Measured Brillouin gain as a function of frequency offset between pump and signal, and of time. The phase-coded B-OCDA setup was adjusted to monitor the Brillouin gain spectrum in a 2 cm-wide hot-spot. Unlike Fig. 7, the delay of the Brillouin signal was stabilized through closed-loop feedback to the wavelength of the sensor laser. The Brillouin gain spectrum remained that of the hot-spot throughout the measurements. Bottom – Wavelength of the Brillouin sensor laser source λ_2 (left-hand axis), and the implied thermal drift in the path length of the 25 km-long delay line (right-hand axis), as a function of time. Thermal drift on the order of 9 cm is observed, which is several times larger than the extent of the hot-spot. SBS: stimulated Brillouin scattering.

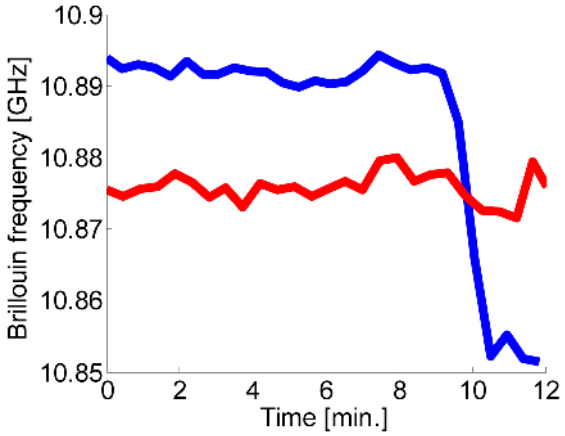

Fig. 9. Measured Brillouin frequency shifts as a function of time. The phase-coded B-OCDA setup was adjusted to monitor the location of a 2 cm-wide hot-spot. Thermal drift in a 25 km-long delay line incorporated in the setup leads to incorrect interrogation after 10 minutes of free-running operation (blue). Thermal drift is overcome with closed-loop, stabilized delay (red).

#247446 Received 5 Aug 2015; revised 20 Sep 2015; accepted 7 Oct 2015; published 20 Oct 2015

5. Discussion

This work addressed the stabilization of thermal drifts in long fiber delay lines, using chromatic dispersion. The output RF phase of a delayed control sine wave was monitored, and used to adjust the wavelengths of tunable laser sources so that delay variations due to temperature and chromatic dispersion canceled out. Residual delay variations of sine waves along 18 km of fiber were reduced to few ps. The obtained performance is analogous to temperature stabilization to within 0.01 °C.

The current work extends over previous reports [19,20], in several respects: a) The input waveform to-be-delayed and the control sine wave are carried over light from separate tunable lasers, at distinctly different wavelengths. The two are therefore separated in the optical domain, and no restrictions are imposed on their RF spectra. b) An extended analysis of the stabilized delay performance is provided. A figure of merit is proposed, in terms of the extent of delay, the range of temperature variations that can be accommodated, and the residual delay fluctuations. An upper bound on attainable performance is established, in terms of the specifications of the tunable laser sources used. c) The distribution of broadband LFM waveforms, which are a mainstay of many radar systems, is demonstrated with reduced delay variations. Lastly, d) the long delay that is required as part of certain types of high-resolution distributed Brillouin sensors is successfully stabilized, allowing for correct interrogation of a localized hot-spot in the presence of significant thermal drift.

In addition to thermal drift, delay along the fiber may also be affected by structural and acoustic vibrations. These were not compensated for in this work, as their frequencies exceed the narrow bandwidth of the specific feedback embodiment used in the current setup. However, this restriction is not fundamental: broader feedback bandwidth was implemented in [19,20], and can be incorporated in the scheme proposed in this work as well, given suitable hardware. Note that in practical applications structural and acoustic vibrations are likely to affect short sections of the fiber only. Vibrations typically modify the delay on the scale of the optical wave period, rather than the periods of radio-frequency wavelengths.

An optical bandwidth of at least twice the control tone frequency must be allocated to the control channel. A single control channel can provide the feedback necessary for stabilizing the delay of multiple optical carriers in wavelength division multiplexing transmission. The separation between the wavelengths of the control and user channels must exceed the sum of the user waveform bandwidth and the control tone frequency, and should also maintain a sufficient guard-band to accommodate the finite transition bandwidth of optical filters. Typically, a wavelength separation of 1 nm would be sufficient. Note that the corrections to both wavelengths are comparable (with second-order differences due to dispersion slope as discussed in section 2). Therefore, the proper wavelength separation between channels would be maintained during operation.

In conclusion, the obtained results demonstrate the applicability of the proposed delay stabilization technique to the processing of broadband microwave signals, as part of larger, more complex systems.

Acknowledgment

The authors thank N. Gilboa for his assistance with the experiments.

#247446 Received 5 Aug 2015; revised 20 Sep 2015; accepted 7 Oct 2015; published 20 Oct 2015